Impact of valence states on the superconductivity of iron telluride and iron selenide films with incorporated oxygen

D. Telesca, Y. Nie, J. I. Budnick, B. O. Wells, and B. Sinkovic

Impact of Valence States on Superconductivity of Oxygen Incorporated Iron Telluride and Iron Selenide Films

D. Telesca[1,2], Y. Nie [2,3], J. I. Budnick[2,3], B. O. Wells[2,3], and B. Sinkovic[2]

[1] *Space Vehicles Directorate, Air Force Research Lab (AFRL), Kirtland AFB, NM 87117*
[2]*Department of Physics, University of Connecticut, Storrs, CT 06269, USA*
[3]*Institute of Materials Science, University of Connecticut, Storrs, CT 06269-3136, USA*
(Received; published)

We report on the local electronic structure of oxygen incorporated FeTe and FeSe films and how this relates to superconductivity observed in these films. In the case of FeTe, initially grown films are measured to be non-superconducting, but become superconducting following oxygen incorporation. In FeSe the opposite happens, initially grown films are measured to be superconducting, but experience a quenching of superconductivity following oxygen incorporation. X-ray Photoemission and Total Fluorescence Yield (TFY) X-ray absorption experiments show that oxygen incorporation changes the initial Fe valence state in both the initially grown FeTe and FeSe films to mainly Fe^{3+} in the oxygen incorporated films. In contrast we observe that while Te moves to a mixed Te^0/Te^{4+} valence state, the Se always remains Se^0. This work highlights how different responses of the electronic structure by the respective chalcogenides to oxidation could be related to the mechanisms which are inducing superconductivity in FeTe and quenching superconductivity in FeSe.

The discovery of superconductivity in the iron pnictide $LaFeAsO_{1-x}Fe_x$[1] (denoted as 1111 compound) has led to the intense investigation of other Fe based superconductors. Hsu et al. discovered superconductivity in FeSe (Tc = 8 K[2]) which has a simple PbO-type structure and a similarity to the critical FeAs$_4$-tetrahedra layers found in all iron-based superconductors. The critical temperature was increased through the partial substitution of Te for Se to a maximum value of T_c = 14 K in $FeSe_xTe_y$ (x=y=0.5)[3] and through the application of high pressure, achieving Tc = 37 K.[4] It has been found that superconductivity disappears at y = 1 in FeTe.[5,6] In addition, it was demonstrated that oxygen poisoning of $Fe_{1.01}Se$ results in a less sharp superconducting transition compared to the sharper transition of oxygen free $Fe_{1.01}Se$.[7]

Due to the isostructural and isoelectronic nature of FeSe and FeTe, it has been surprising that no superconductivity has been observed in single crystal FeTe. Y. Mizuguchi et al.[8] have demonstrated that post growth oxygen annealing is an effective method to induce superconductivity in bulk polycrystalline $FeTe_{1-x}S_x$, but attempts to induce superconductivity in oxidized bulk polycrystalline FeTe were unsuccessful. We recently reported superconductivity in the FeTe film system by the incorporation of oxygen through post growth oxygen annealing.[9] Other reports of FeTe films exhibiting superconductivity also exist in the literature.[10,11]

The question of what parameters control the appearance of superconductivity in the iron superconductors is under intense study. Key ingredients considered include the doping level, the detailed crystal structure, and the relationship to long range ordered magnetism. It has been demonstrated that the tetragonal to orthorhombic structural transition and the long-range antiferromagnetic transition must both be suppressed before the optimum T_c is obtained in any of the FeAs-based systems.[12] This suggests that superconductivity and long-range antiferromagnetic ordering strongly interact, and in fact compete with each other.[13] Studies furthering the understanding of this issue were performed on the $Ba(Fe_{1-x}M_x)_2As_2$ (M = Co, Ni, Rh)

systems which have phase diagrams[14] that show regions where superconductivity and long-range antiferromagnetic order appear to coexist.[13] A relationship between superconductivity and magnetism has also been demonstrated in the Fe-chalcogenide superconductors.[15] The effect of oxygen incorporation into non-superconducting FeTe and superconducting FeSe adds important information on the underlying phase diagram for superconductivity in this family of compounds.

In this work we report changes to the local electronic structure of FeSe and FeTe films resulting from oxygen incorporation. These changes are examined in light of the corresponding resistivity measurements which show a suppression of the superconducting transition in oxygen incorporated FeSe films and the onset of superconductivity in oxygen incorporated FeTe films. X-ray absorption (XAS) and X-ray Photoemission (XPS) measurements indicate that the Fe of both parent films experiences a similar nominal valence change whereas the valence states of the respective chalcogenides (Te, Se) have different responses.

FeTe and FeSe films, 80 ± 15 nm thick, were grown and characterized in the same manner as described in our previous work.[9] Te and Se films were grown on Si (100) substrates by PLD, using a Te (Se) target pressed from the same powder used in the FeTe (FeSe) target. The base pressure of the PLD system was around $7x10^{-8}$ torr during deposition of the Te film and the substrate temperature was kept at 100°C in a vacuum of less than $2x10^{-7}$ torr. After deposition, all films were cooled down to room temperature at a rate of 4°C/min in vacuum. XAS experiments were performed at the National Synchrotron Light source at the U4B beam line. All the XAS data were taken with normal photon beam incidence, with a beam spot of 1x3 mm^2 and photon energy resolution of 0.34 eV for the Fe-L edges and 0.42 for the Te-M edges. All XAS data were normalized by the photon flux recorded with a gold mesh. The XAS spectra were recorded simultaneously in total florescence yield (TFY) and total electron yield (TEY) modes, for probing the bulk and the surface of the films, respectively. All spectra have been

relatively energetically aligned from reference spectra that were simultaneously recorded during all measurements. X-ray Photoemission Spectroscopy (XPS) experiments were performed at the University of Connecticut using laboratory Al-K-α X-rays without monochromator and Scienta SES 100 electron energy analyzer with an overall energy resolution of about 1.5 eV, at a pass energy of 50 eV.
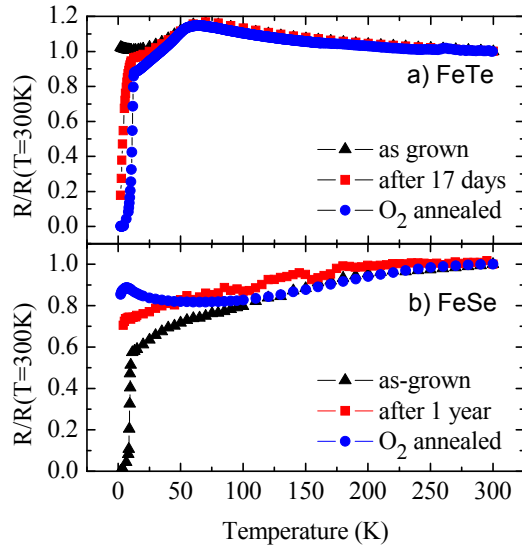
Figure 1: Resistivity measurements normalized to the value at 300 K for a) FeTe films with various amounts and types of oxygen exposure and b) FeSe films with various amounts and types of oxygen exposure

We first describe the transport state of the two Fe-chalcogenide films associated with different oxidation treatments. Figure 1 a) and b) show resistivity measurements of the FeTe and FeSe films, respectively. As was observed in our previous work[9] and shown in Figure 1 by the solid triangles, initially grown FeTe films exhibit a weekly metallic behavior. However, when the films incorporate enough oxygen, they become superconducting. Oxygen incorporation is accomplished either through a sufficient length of ambient air exposure[9] (solid squares) or low temperature oxygen annealing (solid circles), which consists of exposing the films to 100 mTorr of O_2, for 30 min, at 100°C. The opposite trend in transport behavior is observed in the isostructural FeSe film system. In Figure 1b) the solid black triangles show that initially grown FeSe films are superconducting, with a Tc ~ 8 K, consistent with PLD films grown in other work[16]. Oxygen incorporated FeSe films, experience a suppression of the superconducting state, either through long term exposure to air or O_2 annealing.
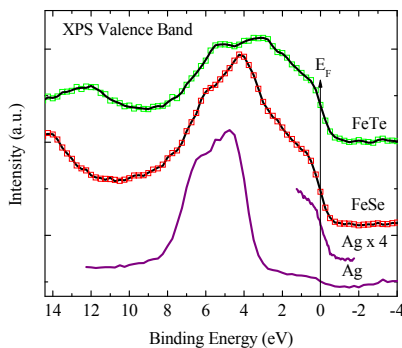
Figure 2: XPS valence band spectra for an unexposed FeTe film and Ag capped, unexposed FeTe film. For the spectrum from the FeTe film, open squares are raw data and the solid line is from a fitting function.

Core level XPS spectra from FeTe and FeSe films grown and measured in-vacuo establish the surface valence states in films unexposed to oxygen. The binding energies of the XPS spectra were calibrated from the Fermi Energy of a silver-capped, unexposed FeTe(Se) film, using the valence band spectrum shown in Figure 2. In addition, the binding energy positions for the same film(s) were calibrated from adventitious carbon at a binding energy of 284.6 eV and were found to yield equivalent binding energies as when calibrated using the Fermi Energy. The surface of the FeTe(Se) films are predominantly not metallic following any exposure to oxygen, so XPS spectra from oxygen incorporated FeTe(Se) films were calibrated by the latter method.

We examined the Fe-2p, Te-3d, and Se-3d regions to determine the valence states of the Fe, Te and Se in un-exposed FeTe(Se) films. Figure 3a) compares the Fe-2p spectra from the unexposed FeTe(Se) films to a spectrum from a metallic Fe reference film. The binding energy values of the Fe-2p$_{3/2}$ peak at 706.8 eV and Fe-2p$_{1/2}$ peak at 720.2 eV (indicated by the arrows in Figure 3) in both the FeTe and FeSe spectra are in excellent agreement with the Fe-2p binding energy values of the metallic reference, as well as in excellent agreement with the literature for Fe[17], as well as PLD grown FeSe films[18,19].
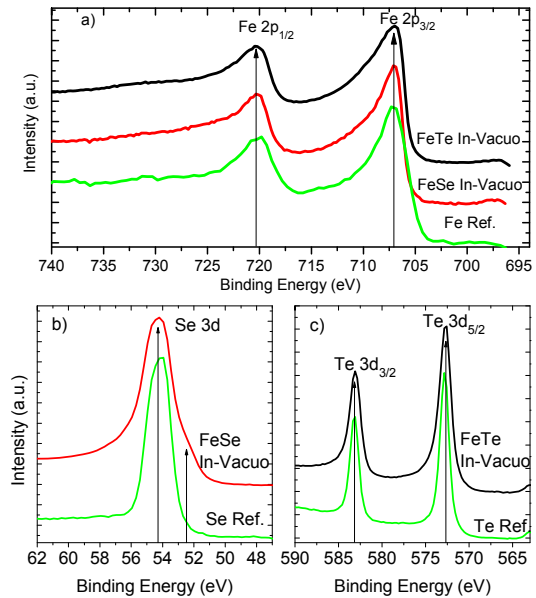
Figure 3: XPS spectra from FeTe and FeSe films grown and measured in-vacuo compared to various reference spectra. a) Fe-2p region comparing the spectra from the in-vacuo FeTe and FeSe films to a spectrum from a metallic Fe reference film. b) Se-3d region comparing the spectrum from the in-vacuo FeSe film to the spectrum from a Se reference film. b) Te-3d region comparing the spectrum from the in-vacuo FeTe film to the spectrum from a Te reference film.

The binding energy positions were obtained from voigt functions fit to the spectra in Figure 3a), following the subtraction of a Shirley background. These binding energy values, in combination with the absence of the well-known[20,21] and distinct higher valence satellite features of Fe, indicate that the surface Fe in both un-exposed FeTe and FeSe films has a valence of zero. Figure 3b) compares the Se-3d spectrum from the un-exposed FeSe film to the spectrum from a Se reference film. The 54.3 eV binding energy of the peak maximum in both spectra is in excellent agreement with the literature for zero valence Se[22] as well PLD grown FeSe films[18,19]. The additional shoulder in the spectrum from the un-exposed FeSe film at 52.5 eV corresponds to the Fe-3p peak of zero valence Fe[23]. Figure 3c) compares the Te-3d spectrum from the un-exposed FeTe film to the spectrum from the Te reference film. The Te-3d$_{5/2}$ peak maximum at a

binding energy of 572.8 eV and Te-$3d_{3/2}$ peak maximum at a binding energy of 583.2 eV in both spectra are consistent within the range of binding energies typically assigned to metallic Te[24,17]. We note the absence of any features in the spectrum from the un-exposed FeTe film at 576.1 eV and 586.7 eV which are known to originate from Te^{4+} states in TeO_2[25]. This demonstrates that the Te is zero valence at the surface of the unexposed FeTe films. Thus, the core level XPS spectra in Figure 3 demonstrate that the surface valence states of Fe and both chalcogenides in un-exposed FeTe and FeSe films are all zero. These results, correlated with the results from Figure 1, show that un-exposed FeTe films are non-superconducting, while un-exposed FeSe films are superconducting, yet both films exhibit the same surface electronic structure.

In our previous work, we demonstrated low temperature oxygen annealing (100 mTorr of O_2 at 100°C for 30 minutes) as an effective technique to induce superconductivity in FeTe films (see Figure 1).[9] In addition, we reported for the first time in Figure 1 that the same oxygen annealing procedure will suppress the superconducting state in FeSe films. To determine the resulting surface valence states XPS spectra from unexposed FeTe and FeSe films were measured following oxygen annealing. Figure 4 shows the Fe-2p, Se-3d and Te-3d XPS spectra from unexposed FeTe and FeSe films before and after oxygen annealing treatments, labeled with their measured transport states (superconducting = SC, non-superconducting = NSC).
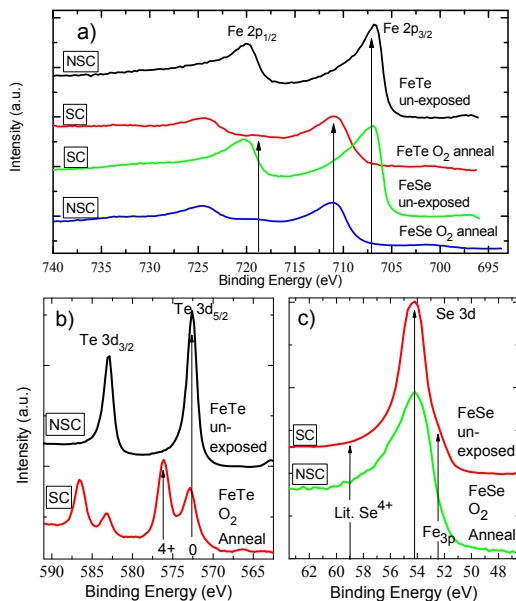
Figure 4: XPS spectra from FeTe and FeSe films grown and measured in-vacuo. a) Fe-2p region comparing the spectra from the un-exposed FeTe and FeSe films to the spectra following in-vacuo O_2 annealing of the respective films. b) Te-3d region comparing the spectrum from the un-exposed FeTe film to the spectrum following O_2 annealing of the film. c) Se-3d region comparing the spectrum from the un-exposed FeSe film to the spectrum following O_2 annealing of the film.

We first consider changes to the local electronic structure in the FeTe film. The Fe-2p XPS spectra from the FeTe film before and after oxygen annealing is shown in Figure 4a). The spectra indicate a change in Fe valence from zero in the un-exposed film (as determined from Figure 3), to Fe^{3+} following oxygen annealing. This can be seen by the binding energy shift of the Fe-$2p_{3/2}$ peak from 706.8 eV to 710.8 eV, as well as by the appearance of a satellite feature at 718.8 eV. These spectral characteristics are consistent with the Fe-$2p_{3/2}$ binding energy position and satellite feature originating from Fe^{3+} found in bulk Fe_2O_3.[20,21] The Te-3d XPS spectra in Figure 4b) clearly show the Te valence changes from initially zero to a mixed valence

state by the appearance of peaks at 576.1 eV and 586.6 eV. The binding energy positions of these peaks are consistent with the Te-3d peaks originating from Te^{4+} found in bulk TeO_2.[26] The measured transport states noted in Figure 4 show that the surface valence of both Fe and Te are zero in the non-superconducting FeTe film and change to Fe^{3+} and mixed Te^0/Te^{4+} in the superconducting state.

In the FeSe film, the change in Fe valence is similar to the change observed in the FeTe film. Again, this is determined in Figure 3a) from the binding energy shift of the Fe-$2p_{3/2}$ peak from 706.9 eV to 710.9 eV, as well as by the appearance of a satellite feature at 718.8 eV. Interestingly, the Se-3d spectrum from the oxygen annealed FeSe film exhibits neither a shift of the peak maximum nor appearance of any structure associated with other Se valence states. Specifically, there is no structure located at a binding energy of 59 eV where Se^{4+} would be located.[27] Although XPS is a surface sensitive technique, the complete absence of any higher valence feature of Se in the XPS spectra we take as evidence that valence changes in the bulk of the film are unlikely to occur. Direct measurement of the bulk electronic structure using bulk sensitive TFY-XAS measurements is discussed below, however, the Se XAS edges were outside of the photon energy range available at the U4B beam line. We believe this qualitative observation can be interpreted as clear evidence that the Se valence remains zero throughout the bulk of the FeSe films.

As was noted in Figure 3, the shoulder at 52.5 eV in the spectrum from the un-exposed FeSe film corresponds to the Fe-3p peak of Fe^0.[28] The Se 3d spectrum from the O_2 annealed FeSe film exhibits a reduction in intensity at 52.5 eV and increase in intensity at 56 eV corresponding to the change of Fe^0 to Fe^{3+} observed in Figure 4a).[28] In contrast to the FeTe film, the measured transport states noted in Figure 4 show that the surface valence of both Fe and Se are zero in the *superconducting* FeSe film. When superconductivity is suppressed in the oxygen annealed FeSe film, only the Fe valence changes to Fe^{3+}, while the chalcogenide valence remains the same.

To determine that the observed surface valence changes were also intrinsic properties related to the appearance and suppression of superconductivity in these films, the bulk electronic structures of both non-superconducting and superconducting FeTe and FeSe films were probed with X-ray Absorption Spectroscopy (XAS) using Total Fluorescence Yield (TFY). With a probing depth on the order of the film thicknesses, ~100 nm, TFY-XAS is a well suited probe of the bulk electronic structure of these films.

Our previous work reported that in addition to oxygen annealing, a critical exposure time to air has the equivalent effect on the bulk transport properties of the films (see Figure 1).[9] Thus, in the following studies of the bulk electronic structure, the effect of both methods for inducing and suppressing superconductivity were examined and compared.

The Fe-L edges from an oxygen annealed FeTe(Se) film and an FeTe(Se) film exposed to air for increasing amounts of time are shown in Figure 5a) and b). The measured transport states corresponding to the different statuses of the films have been noted. Spectra from bulk FeO and Fe_2O_3 have been included for comparison.

In-vacuo growth and TFY-XAS measurements of the films was not possible, so to approximate as close to un-exposed FeTe and FeSe films as was possible, the films were transported directly from our growth chamber to the U4B beamline in a vacuum suitcase. However, this resulted in 4 hours of air exposure for the FeTe film and 5 hours for the FeSe film. These times represent the total time starting from the initial exposure of the films (required for mounting at U4B) and ending when the pressure in the XAS measurement chamber, now containing the films, reached ~10^{-9} torr.

Attempts to fit the spectra from the hours-long air-exposed films were made, but could not yield fruitful results since it was impossible to quantify the amount of oxygen in these thin films. To interpret the spectra, we consider the in-vacuo XPS results, which demonstrated zero valence surface Fe in both FeTe and FeSe films and use spectra from bulk iron oxides for spectral comparison. The most correct interpretation that can then be speculated about the Fe valence is that it is a mixture of Fe^0 and Fe^{2+} (with spectral maximum located at 706.4 eV). Separating the contributions of Fe^0 and Fe^{2+} in such a mixed valence state is complicated by the overlap of energy positions of the maxima of Fe^0 and Fe^{2+} at both the Fe-L_3 and $-L_2$ edges as can be demonstrated from experimental spectra of Fe and FeO (see for example T.J. Regan, et al.[29]). However, the contribution from Fe^{2+} can still be detected by the shape of the L_2 edge, having a more extended multiple structure (as for example in FeO) when compared to Fe^0. In addition, there is most likely some contribution of Fe^{3+}, which can be seen as the shoulder located at 708.7 eV (indicated by the arrows in Figure 5). Absolute identification of the bulk valence state of Fe in un-exposed films is important to determine, but being beyond the scope of this work, it is the change of Fe to mostly 3+, discussed below, that we focus on.

FeTe film to one that closely resemble that of bulk Fe_2O_3, as well as drives the oxygen incorporated FeTe film to be superconducting. The change of Fe valence from its initial state, to one that is dominated by Fe^{3+} is also clearly observed in the spectrum from the oxygen annealed film. These results indicate that the majority valence state of iron in FeTe films, made superconducting by two independent methods of oxygen incorporation, is dominated by Fe^{3+}. In contrast, the FeSe film was observed to become non-superconducting by the same oxygen incorporation methods. The Fe-L_3 spectra from the year-long air-exposed and oxygen annealed NSC-FeSe films in Figure 5b) show the peak related to Fe^{3+} at 708.7 eV increasing in intensity as compared to the 5-hour and 3-day air-exposed SC-FeSe films. The two main peaks at the Fe-L_3 edge do not show an intensity ratio similar to that seen in the spectrum from bulk Fe_2O_3. Furthermore, the Fe-L_2 edge is more similar to the Fe-L_2 edge from bulk FeO, indicating a significant presence of Fe^{2+}. Therefore, an oxygen incorporated NSC-FeSe film does not have iron in a mostly Fe^{3+} state. Our observations of the spectra from minimally exposed FeSe films and oxygen incorporated FeSe films are in agreement with the results from bulk FeSe studied by Yang *et al.*[30] and Chen *et al.*[31], as well as with theoretical calculations by Lee *et al.*[32] It is concluded that while the same general trend in Fe valence change is observed in both FeTe and FeSe films, the rate at which these occur are different.

Studies of the local electronic structure at the Te-$M_{4,5}$ edges from NSC- and SC-FeTe films were used to determine the bulk valence state of Te. Figure 6 shows the background subtracted Te-$M_{4,5}$ TFY-XAS spectra from a set of FeTe films. Limited published Electron Energy Loss Spectroscopy (EELS) data indicate that Te^0 has an M_5 edge at ~572 eV and M_4 edge at ~583 eV[33,34] and that the Te^{4+} M_5 and M_4 edges appear at respectively higher photon energies than their corresponding metallic edges[35]. The TEY-XAS spectra from the 4-hour-exposed NSC-FeTe film shows peaks at 576.7 eV and 586.3 eV with smaller features on the higher energy side of each of these peaks. The EELS literature, considered in conjunction with the XPS studies previously discussed, indicate that the Te in the bulk of the 4-hour air-exposed NSC-FeTe film is primarily metallic, with some contribution from higher valence Te states. This may suggest that an in-vacuo grown and measured film would show only metallic Te, but similar to the Fe-L edge XAS, absolute determination of this was beyond the scope of this work. The TFY-XAS spectra of both the 24-days air-exposed and O_2 annealed SC-FeTe films show a dramatic increase of the higher energy peaks at 580.4 eV and 589.9 eV, confirming that a dramatic valence change to mixed Te^0/Te^{4+} occurs through the bulk of the films, in addition to occurring at the surface.

Figure 5: Fe L edge TFY-XAS spectra for a) FeTe films with various amounts and types of oxygen exposure and b) FeSe films with various amounts and types of oxygen exposure
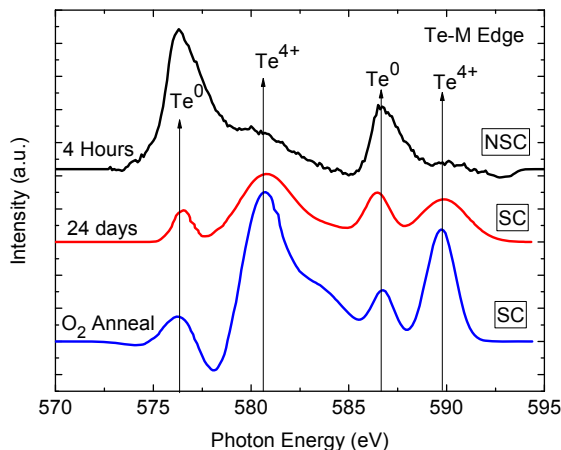
Figure 6: TFY-XAS Te-M edge spectra from a 4-hour air exposed NSC-FeTe film, a 24-days-air exposed SC-FeTe film and an oxygen annealed SC-FeTe film. The spectra in the figure are background subtracted spectra.

The increase in intensity of the peak at 708.7 eV in the spectra from the NSC-FeTe film exposed to air for 4-days and SC-FeSe film exposed to air for 3-days we interpret as an indication of the increase of Fe^{3+} states with continued exposure to air. A significant exposure to air completes this trend and transforms the Fe XAS spectrum from the 24 day air-exposed

In this work, the valence changes of Fe, Te and Se in FeTe and FeSe films were examined as a function of different oxygen incorporation methods and were correlated to their corresponding transport measurements. It was demonstrated that initially grown FeTe is measured to be non-superconducting, with the Fe and Te exhibiting local electronic structures analogous to zero valence Fe and Te. Following sufficient oxygen incorporation, the FeTe films become superconducting and the dominating valence state of Fe changes to nominally Fe^{3+} and Te changes to a mixed Te^0/Te^{4+}. The opposite exists in the FeSe films. Initially grown FeSe films are superconducting with the Fe and Se exhibiting local electronic structures analogous to zero valence Fe and Se. Following sufficient oxygen incorporation, superconductivity is suppressed and the Fe changes valence to nominally Fe^{3+}, while the Se remains zero valence.

The correlation between observed valence changes and the appearance of superconductivity in FeSe and FeTe films is an intriguing phenomenon. In the following, we rule out some trivial explanations for the reported results supporting this observation. Superconductivity in FeSe films and oxygen-incorporated-FeTe films is a bulk phenomenon, as is evidenced by the Meissner effect measured in both systems.[2,9] The possible impact of oxygen incorporation on the FeTe and FeSe compositions was ascertained by Energy Dispersive X-ray (EDX) measurements. Atomic percentages obtained from EDX (accurate to $\pm$ 1%) indicate that the oxygen annealed and air exposed FeTe and FeSe films have no significant deviation from their initial stoichiometry (less than 3% from Fe/X = 1/0.95). These results demonstrate that the onset of superconductivity in FeTe and destruction of superconductivity in FeSe are not the result of sample degradation caused by significant oxygen incorporation. Similarly, the XRD measurements of as-grown and oxygenated FeTe and FeSe films show no change in overall structure and a small change in the lattice constant. Furthermore, the onset and disappearance of superconductivity does not appear to be a specifically film related effect; the films are fully relaxed. Finally, the preliminary DFT calculations on both FeTe and FeSe suggest a common O interstitial site, indicating again similarity of the two systems.[36]

The most notable difference between SC-FeTeOx and NSC-FeSeOx is the chalcogenide valence. However, we know of no particular reason this might induce or suppress superconductivity and we know of no similar effect in the Fe pnictides. The fundamental observation that incorporated oxygen creates superconductivity in FeTe films and destroys it in FeSe films, however, presents a possible test bed for identifying the controlling factor responsible for superconductivity in these isostructural and isoelectronic materials.

1   Y. Kamihara, T. Watanabe, M. Hirano, and H. Hosono, J. Am. Chem. Soc 130, 3296 (2008).
2   F.-C. Hsu, J.-Y. Luo, K.-W. Yeh, T.-K. Chen, T.-W. Huang, P. M. Wu, Y.-C. Lee, Y.-L. Huang, Y.-Y. Chu, D.-C. Yan, and M.-K. Wu: Proc. Nati. Acad. Sci. 105 (2008) 14262.
3   M.K. Wu, F.C. Hsuc, K.W. Yeh, T.W. Huang, J.Y. Luo, M.J. Wang, H.H. Chang, T.K. Chen, S.M. Rao, B.H. Mok, C.L. Chen, Y.L. Huang, C.T. Ke, P.M. Wu, A.M. Chang, C.T. Wu and T.P. Perng, Physica C 469 (2009), p. 340.
4   S. Margadonna, Y. Takabayashi, Y. Ohishi, Y. Mizuguchi, Y. Takano, T. Kagayama, T. Nakagawa, M. Takata, and K. Prassides: Phys. Rev. B 80 (2009) 064506.
5   K.-W. Yeh, T.-W. Huang, Y.-L. Huang, T.-K. Chen, F.-C. Hsu, P. M. Wu, Y.-C. Lee, Y.-Y. Chu, C.-L. Chen, J.-Y. Luo, D.-C. Yan, and M.-K. Wu: Europhys. Lett. 84 (2008) 37002.
6   M. H. Fang, H. M. Pham, B. Qian, T. J. Liu, E. K. Vehstedt, Y. Liu, L. Spinu, and Z. Q. Mao: Phys. Rev. B 78 (2008) 224503
7   T. M. McQueen, Q. Huang, V. Ksenofontov, C. Felser, Q. Xu, H. Zandbergen, Y. S. Hor, J. Allred, A. J. Williams, D. Qu, J. Checkelsky, N. P. Ong, and R. J. Cava, Phys. Rev. B, 79, 014522 (2009).
8   Y. Mizuguchi, K. Deguchi, S. Tsuda, T. Yamaguchi, Y. Takano: arXiv: 1003.2059v2.
9   Y. Nie, D. Telesca, J.I. Budnik, B. Sinkovic and B.O. Wells, Phys. Rev. B, 82, (2010) 020508 (R).
10   Y. Han, w. Y. Li, L. X. Cao, X. Y. Wang, B. Xu, B. R. Zhao, Y. Q. Guo, and J. L. Yang, Phys. Rev. Lett., 104 (2010) 017003.
11   W. Si, Q. Jie, L. Wu, J. Zhou, G. Gu, P. D. Johnson, and Q. Li, Phys. Rev. B, 81 (2010) 092506.
12   J. Zhao, Q. Huang, C. de la Cruz, S. Li, J. W. Lynn, Y. Chen, M. A. Green, G. F. Chen, G. Li, Z. Li, J. L. Luo, N. L. Wang, and P. Dai, Nature Mater. 7, 953 (2008).
13   D. C. Johnston, arXiv:1005.4392v2, August (2010).
14   S. Nandi, M. G. Kim, A. Kreyssig, R. M. Fernandes, D. K. Pratt, A. Thaler, N. Ni, S. L. Bud'ko, P. C. Canfield, J. Schmalian, R. J. McQueeney, and A. I. Goldman, Phys. Rev. Lett. 104, 057006 (2010).
15   A. Martinelli, A. Palenzona, M. Tropeano, C. Ferdeghini, M. Putti, M. R. Cimberle, T. D. Nguyen, M. Affronte,5 and C. Ritter, Phys. Rev. B, 81 (2010) 094115.
16   T-K. Chen, J-Y. Luo, C-T Ke, H-H. Chang, T-W. Huang, K-W. Yeh, C-C. Chang, P-C. Hsu, C-T. Wu, M-J. Wang, M-K. Wu, Thin Solid Films (2010), doi:10,1016/j.tsf.2010.06.002.
17   C.D. Wagner, W.M. Riggs, L.E. Davis, J.F. Moulder, G.E. Muilenberg, Editor, *Handbook of X-Ray Photoelectron Spectroscopy: A Reference Book of Standard Spectra for Identification and Interpretation of XPS Data*, Perkin-Elmer Corp., Physical Electronics Division, Minnesota, USA (1979)
18   T.-K. Chen, J.-Y. Luo, C.-T. Ke, H.-H. Chang, T.-W. Huang, K.-W. Yeh, C.-C. Chang, P.-C. Hsu, C.-T. Wu, M.-J. Wang, M.-K. Wu Thin Solid Films 519 (2010) 1540-1545.
19   A. Tsukada, K. E. Luna, R. H. Hammond, M. R. Beasley, J.F. Zhao, S.H. Risbud, Appl. Phys. A 104 (2011) 311-318.
20   S. J. Roosendaal, I. A. M. E. Giebels, A. M. Vredenberg and F. H. P. M. Habraken, Surf. Interface Anal. 26, (1998) 758-765.
21   P.C.J. Graat. and M.A.J. Somers, Applied Surface Science 100-101 (1996) 36.
22   Ming-Zhe Xue and Zheng-Wen Fu, *Electrochim. Acta* 52 (2006), p. 988.
23   R. J. Lad and V. E. Henrich, Phys. Rev. B, 39 (1989) 13,478.
24   W.P. Zhou, L.A. Kibler, D.M. Kolb, Electrochimica Acta 47 (2002) 4501 - 4510.
25   O.A. Balitskii, W. Jaegermann, Materials Chemistry and Physics 97 (2006) 98–101.
26   O.A. Balitskii, W. Jaegermann, Materials Chemistry and Physics 97 (2006) 98–101.
27   R. Würz, M. Rusu, T. Schedel-Niedrig, M.C. Lux-Steiner, H. Bluhm, M. Hävecker, E. Kleimenov, A. Knop-Gericke and R. Schlögl, *Surf. Sci.* 580 (2005), pp. 80–94.
28   R. J. Lad and V. E. Henrich, Phys. Rev. B, 39 (1989) 13,478.
29   T.J. Regan, H. Ohldag, C. Stamm, F. Nolting, J. Lüning, J. Stöhr and R.L. White, *Phys. Rev. B* 64 (2001), p. 214422.
30   W. L. Yang, A. P. Sorini, C-C. Chen, B. Moritz, W.-S. Lee, F. Vernay, P. Olalde-Velasco, J.D. Denlinger, B. Delley, J.-H. Chu, J.G. Analytis, I.R. Fisher, Z. A. Ren, J. Yang, W. Lu,

Z. X. Zhao, J. van den Brink, Z. Hussain, Z.-X. Shen, and T. P. Devereaux, Phys. Rev. B, **80** (2009) 014508.

[31] C. L. Chen, S. M. Rao, C. L. Dong, J. L. Chen, T. W. Huang, B. H. Mok, M.C. Ling, W. C. Want, C. L. Chang, T. S. Chan, J. F. Lee, J.-H. Guo and M. K. Wu, Euro. Phys. Lett. **93** (2011) 47003.

[32] K.-W. Lee, ZV. Pardo and W. E. Pickett, Phys. Rev. B, **78** (2008) 174502.

[33] *X-ray Data Booklet*; Lawrence Berkeley Laboratory: Berkeley, CA, 2001.

[34] S.A. Song, W. Zhang, H. Sik Jeong, J.-G. Kim, Y.-J. Kim, Ultramicroscopy **108** (2008) 1408.

[35] N. Jiang and J. C. H. Spence, Phys. Rev. B., **70**, 014112 (2004).

[36] Y.F. Nie, J.I. Budnick, R. Ramprasad, B.O. Wells, in preparation.